ChemComm

COMMUNICATION

View Article Online
View Journal | View Issue

Open Access Article. Published on 07 April 2016. Downloaded on 2/10/2026 8:45:29 AM.
This article is licensed under a Creative Commons Attribution 3.0 Unported Licence.

Cite this: *Chem. Commun.*, 2016, 52, 6375

Received 10th March 2016,
Accepted 7th April 2016

DOI: 10.1039/c6cc02121b

www.rsc.org/chemcomm

$Ba_4Ru_3O_{10.2}(OH)_{1.8}$: a new member of the layered hexagonal perovskite family crystallised from water†

Craig I. Hiley,[a] Martin R. Lees,[b] David L. Hammond,[b] Reza J. Kashtiban,[b] Jeremy Sloan,[b] Ronald I. Smith[c] and Richard I. Walton*[a]

A new barium ruthenium oxyhydroxide $Ba_4Ru_3O_{10.2}(OH)_{1.8}$ crystallises under hydrothermal conditions at 200 °C: powder neutron diffraction data show it adopts an 8H hexagonal perovskite structure with a new stacking sequence, while high resolution electron microscopy reveals regions of ordered layers of vacant Ru sites, and magnetometry shows antiferromagnetism with T_N = 200(5) K.

Oxides of the second- and third-row transition elements are of topical interest for their exotic magnetic properties, which have been rather less explored compared to their first-row analogues. The range of striking magnetic and electronic properties is exemplified by ruthenates, such as superconductivity in Sr_2RuO_4,[1] ferromagnetism in $SrRuO_3$,[2] antiferromagnetism persisting to 560 K in $SrRu_2O_6$[3] and non-Fermi-liquid behaviour in $La_4Ru_6O_{19}$.[4] Complex ruthenium oxides are also of interest in heterogeneous catalysis,[5,6] and for electrocatalytic splitting of water.[7] The structural chemistry of barium ruthenates is known already to be particularly extensive, and in this family there is a notable propensity to adopt hexagonal perovskite structures. These consist of layers of hexagonal close-packed [BaO_3] units with Ru atoms occupying a fraction of the octahedral interstices.[8,9] Layers are stacked along the *c*-axis such that octahedra are linked in either a corner-sharing manner (as in the cubic perovskite, denoted *c*) or in a face-sharing manner (hexagonal close packing, *h*), which may be stabilised by metal–metal bonding. Whilst some of these phases are stoichiometric, namely the 4H-, 9R- and 10H-$BaRuO_3$ variants,[10–12] hexagonal perovskites with compositional variation have also been discovered. Deviation from the ideal ABO_3 composition has been observed in the form of both Ru deficiency (as observed in $Ba_5Ru_2O_{10}$ and $Ba_5Ru_2O_9(O_2)$[13,14]) and substitution of Ru for other metals (Li, Na, Mg, Zn;[15] Ni, Co, Zn[16]).

When preparing new complex ruthenates, highly oxidising environments are often required to access oxidation states of Ru higher than +4, and, indeed, to prevent reduction to Ru metal, however high oxygen pressure at elevated temperatures can lead to formation and volatilisation of considerable quantities of $Ru^{VIII}O_4$ making control of composition challenging.[17] Low temperature synthesis techniques that can stabilise highly oxidised Ru, such as molten salt flux crystal growth[18] and hydrothermal crystallisation,[19] are therefore attractive propositions for the isolation of complex ruthenium oxides. Recently we reported the unique structure of $Ba_2Ru_3O_9(OH)$, an oxyhydroxide prepared by a hydrothermal reaction.[20] We demonstrate herein that by simply altering the ratio of the two reagents, this synthetic procedure yields a structurally unrelated, 8H-hexagonal perovskite phase $Ba_4Ru_3O_{10.2}(OH)_{1.8}$, which contains a new stacking sequence, and regions of vacancy ordering.

Phase-pure $Ba_4Ru_3O_{10.2}(OH)_{1.8}$ was prepared by the hydrothermal reaction of BaO_2 and $KRuO_4$ at 200 °C for 24 hours in a 2 : 1 ratio (*i.e.* an excess of Ba). A silver-grey powder was recovered by suction filtration and washed with 0.1 M HCl to remove any $Ba(OH)_2$ or $BaCO_3$ byproducts, as we found necessary in earlier work on other oxides.[20] The powder X-ray diffraction pattern of the new phase was indexed to a hexagonal unit cell with lattice parameters a = 5.79905(7) Å, c = 18.7562(5) Å, similar to those of the barium ruthenate 8H-perovskites $Ba_4Ru_3NaO_{12}$[15] and $Ba_2Ru_5O_{10}$.[21] ICP measurements give a Ba : Ru 1.33(1) : 1 ratio, and no K was detected (detection limit 10 ppm). A structural solution was initially found by a Monte Carlo optimisation in direct space using the software FOX,[22] and a Rietveld refinement of this structure against time-of-flight powder neutron diffraction data (PND, GEM, ISIS; Fig. 1(a)) was carried out in GSAS[23] implemented using EXPGUI.[24] The best fit was obtained in the space group $P6_3/mmc$.

The structure of $Ba_4Ru_3O_{10.2}(OH)_{1.8}$ consists of an eight-layer stacking sequence, $(chhh)_2$ (Fig. 2(a)), with chains of four face-sharing octahedral sites (Table 1 and Fig. 1(b)). However, the Ru2 site, which lies within the two central octahedral sites of the quasi-tetrameric chains (Fig. 1(c)), is only half-occupied. Examination of high angle annular dark field images obtained in scanning

[a] *Department of Chemistry, University of Warwick, Coventry, CV4 7AL, UK. E-mail: r.i.walton@warwick.ac.uk*
[b] *Department of Physics, University of Warwick, Coventry, CV4 7AL, UK*
[c] *ISIS Facility, Rutherford Appleton Laboratory, Harwell Campus, Didcot, Oxfordshire, OX11 0QX, UK*

† Electronic supplementary information (ESI) available: Further experimental details, characterisation data and supplementary materials. See DOI: 10.1039/c6cc02121b

Open Access Article. Published on 07 April 2016. Downloaded on 2/10/2026 8:45:29 AM.
This article is licensed under a Creative Commons Attribution 3.0 Unported Licence.

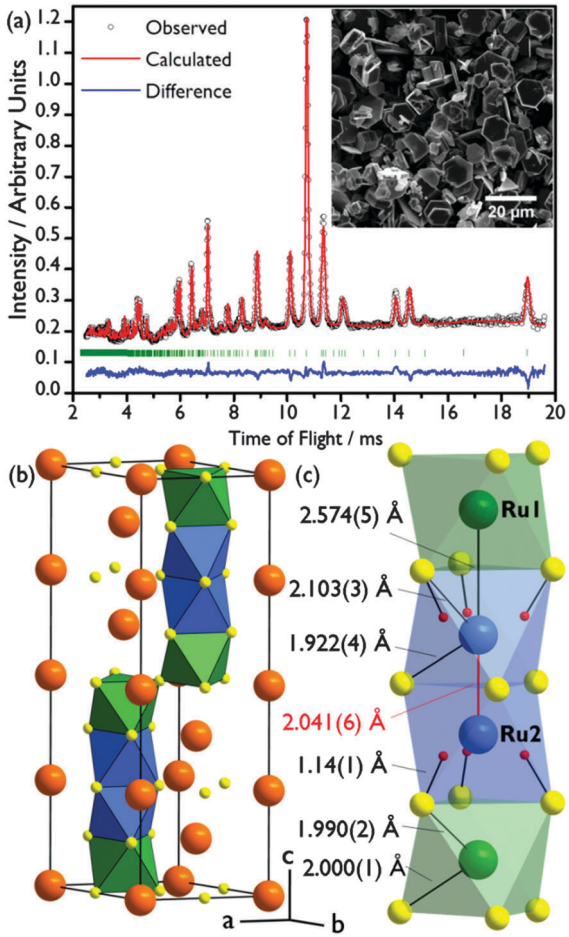

Fig. 1 (a) Rietveld fit to powder neutron diffraction (GEM Bank 4) with scanning electron micrograph inset. (b) Representation of the unit cell of $Ba_4Ru_3O_{10.2}(OH)_{1.8}$ with Ba atoms in orange, oxygen atoms in yellow, fully occupied octahedral sites in green and half-occupied octahedral sites in blue. (c) One chain of four octahedral Ru sites with refined bond lengths labelled. H sites in red.

Table 1 Final refined atomic parameters for $Ba_4Ru_3O_{10.24(4)}(OH)_{1.76(4)}$. Space group $P6_3/mmc$; a = 5.79905(7) Å, c = 18.7562(5) Å. Refined from PND, χ^2 = 1.92, R_p = 2.01%, R_{wp} = 2.61%. BVS: bond valence sum *O3 BVS dependent on local environment. See text and ESI for further details

Atom	x/a	y/b	z/c	Occupancy	ADP/Å^2	BVS
Ba1	0	0	0	1	0.010(1)	2.34
Ba2	0	0	1/4	1	0.015(1)	2.10
Ba3	1/3	2/3	0.1280(2)	1	0.0070(5)	2.32
Ru1	1/3	2/3	0.5584(1)	1	0.0159(4)	4.39
Ru2	1/3	2/3	0.8044(2)	0.5	0.0080(6)	4.41
O1	0.5045(3)	0.0090(6)	1/4	1	0.0151(4)	1.72
O2	1/2	0	0	1	0.0046(2)	2.22
O3	0.1751(2)	0.3502(4)	0.8778(1)	1	0.0129(2)	1.50/2.06/2.09*
H1	0.2349(8)	0.470(2)	0.6741(6)	0.294(6)	0.056(5)	0.59

transmission electron microscopy (HAADF STEM) shows that regions of the sample show extensive vacancy ordering (Fig. 2(b)). A refinement to the powder neutron diffraction using a model in the lower symmetry space group $P6_3mc$ with ordered vacant sites yields a poorer fit to the data (see ESI†), suggesting that although vacancies may order in domains on the nanoscale, on average the Ru2 site is randomly occupied. Whilst the Ru1 site sits on the highly symmetrical octahedral site (Ru–O bond distances in the range 1.990(2)–2.000(1) Å), the Ru2 sits off-centre in an octahedral site, generating three long (2.103(3) Å) and three short (1.922(4) Å) Ru–O distances (Fig. 1(c)). This gives a Ru1–Ru2 bond distance of 2.574(5) Å, a value consistent with an average Ru oxidation state of +4.5–4.75 in barium ruthenates, using the correlation established by Kimber *et al.* in their study of 6H perovskites $Ba_3ARu_2O_9$.[26] A second consequence of the Ru2 site asymmetry is the unphysically short distance between neighbouring Ru2 sites of 2.041(6) Å, indicating that whilst there is no preferential ordering within the quasi-tetrameric chains, there must be exactly one octahedral vacancy per chain. The structure can be compared to the structure adopted in another ruthenate 8H-perovskite, $Sr_4Ru_{3.05}O_{12}$, which also contains partially occupied face-sharing Ru octahedra and, due to the $(ccch)_2$ stacking sequence, also has no Ru–Ru bonding (see ESI†).[25]

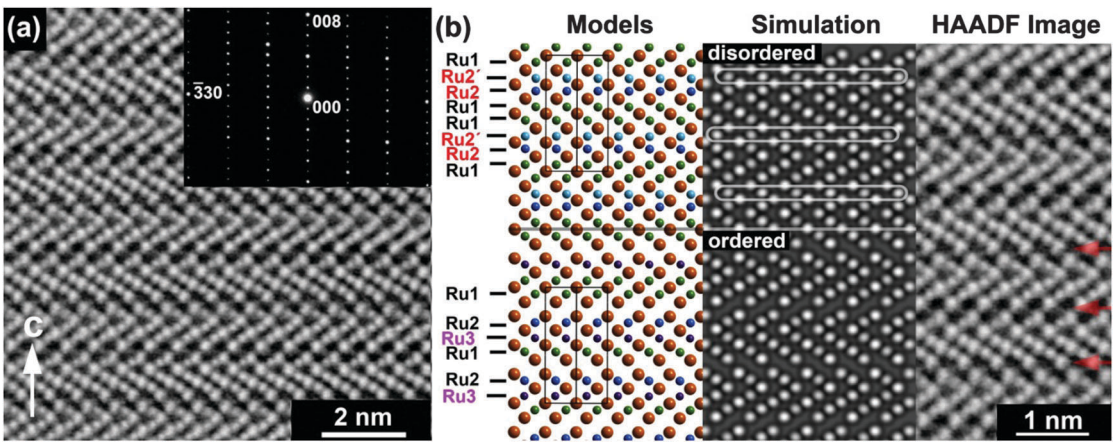

Fig. 2 (a) HAADF STEM image of $Ba_4Ru_3O_{10.2}(OH)_{1.8}$ with inset electron diffraction pattern. (b) Comparison of simulated HAADF images from disordered and ordered Ru vacancies to an experimental HAADF image obtained from a [110] projection. In the disordered simulation partially occupied Ru positions (Ru2′) are indicated by a loop in the simulated image. The diffuse red arrows in the experimental HAADF indicate that these are absent observable by comparison with the 'ordered' simulation.

 This journal is © The Royal Society of Chemistry 2016

Open Access Article. Published on 07 April 2016. Downloaded on 2/10/2026 8:45:29 AM.
This article is licensed under a Creative Commons Attribution 3.0 Unported Licence.

Examination of difference Fourier maps revealed a site containing negative scattering density within these partially occupied octahedra, approximately 1 Å from the O3 site (which is otherwise under-coordinated due to Ru vacancies, Table 1), strongly suggesting the presence of H. This 12-fold site has a refined occupancy of 0.294(6), equivalent to 1.76(4) H per formula unit, giving the refined empirical formula $Ba_4Ru_3O_{10.24(4)}(OH)_{1.76(4)}$ and an O–H bond length of 1.14(1) Å (Fig. 1(c)). The O3 bond valence sum has a range of values, depending on its local environment. When it is bonded to either a Ru2 or H atom the value is close to the expected value of 2 (2.06 and 2.09 respectively). However, in the refined model approximately one in six oxygen atoms is under-coordinated, giving a bond valence sum of 1.50. The high correlation of the H1 and Ru2 atomic parameters led us to consider the possibility that the H1 occupancy is truly 0.5, which would result in O3 BVS much closer to 2. However, refinements carried out with fixed H1 occupancies show a poorer fit to the data, with unphysical refined values for Ru2 and H1 atomic displacement parameters (see ESI†).

Thermogravimetric analysis (TGA) under a N_2 gas flow combined with mass spectrometry (MS) of the evolved gas confirms the presence of structural hydroxide: after a small initial loss of surface adsorbed water from the ~10 μm crystallites (Fig. 1(a)), a mass loss of 1.55% occurs at ~300 °C (Fig. 3(a)), with MS allowing this to be attributed to the loss of H_2O due to the loss of the 1.80 hydroxide groups per formula unit, consistent with the structural model refined from powder neutron diffraction. This also correlates with *in situ* X-ray thermodiffraction data, which show a structural transition at around 300 °C, which must be brought about by dehydroxylation (see ESI†).

Structural hydroxide has been previously observed in metal-deficient perovskites,[27,28] although previously reported examples are typically ReO_3-type structures where the H atoms project into the voids left by unoccupied A-sites. These are significantly larger than the B-site voids observed in $Ba_4Ru_3O_{10.2}(OH)_{1.8}$, explaining the partial occupancy of the H-site (1.8 H per vacant octahedron, compared with 3 in ReO_3-type hydroxides).[27,28] Hydroxylation may be driven by both the highly basic, oxidising synthesis conditions and the unique packing sequence observed in this hexagonal perovskite which necessitates Ru deficiency for steric reasons, leading to hydroxylation of otherwise under-coordinated oxide.

From the refined chemical formula, an average Ru oxidation state of +4.75 is deduced. Ru bond valence sums suggest a similar oxidation state of +4.40, with little difference between the two crystallographically distinct sites despite the large asymmetry seen in Ru2 (Table 1). X-ray absorption near edge structure (XANES) spectroscopy experiments were undertaken for further evaluation of the Ru oxidation state, with the Ru K-edge XANES spectrum of the $Ba_4Ru_3O_{10.2}(OH)_{1.8}$ compared to spectra of oxides of known oxidation state, Fig. 3(b) (see ESI† for full spectra). Although Ru K-edge XANES has previously been shown to be sensitive to the Ru average oxidation state,[19,29,30] significant core-hole broadening at the Ru K-edge[31] introduces large uncertainty in the measured edge position, and differences in local environment are also known to affect edge position. Despite this, the Ru K-edge position of the standards was found to have a linear relationship with oxidation state, with the $Ba_4Ru_3O_{10.2}(OH)_{1.8}$ K-edge position consistent with Ru oxidation state between 4.70 and 5 (Fig. 3(b)).

A Curie–Weiss law fit to the magnetic susceptibility *versus* temperature data in the paramagnetic region ($250 < T < 400$ K), yields an effective Ru moment, μ_{eff}, of 3.13 μ_B and a Weiss temperature, θ, of −629.2(8) K, indicative of significant antiferromagnetic correlations, Fig. 4. The Ru average valence state of +4.75 suggests a mixture of Ru^{4+} (t_{2g}^4) and Ru^{5+} (t_{2g}^3) ions with spin-only moments of 2.83 μ_B and 3.87 μ_B respectively, which would give an average spin-only moment of 3.64 μ_B in $Ba_4Ru_3O_{10.2}(OH)_{1.8}$. The difference between the spin-only value and μ_{eff} can be explained by a combination of crystalline field and spin–orbit coupling effects, commonly observed in Ru(v) oxides.[20,32,33]

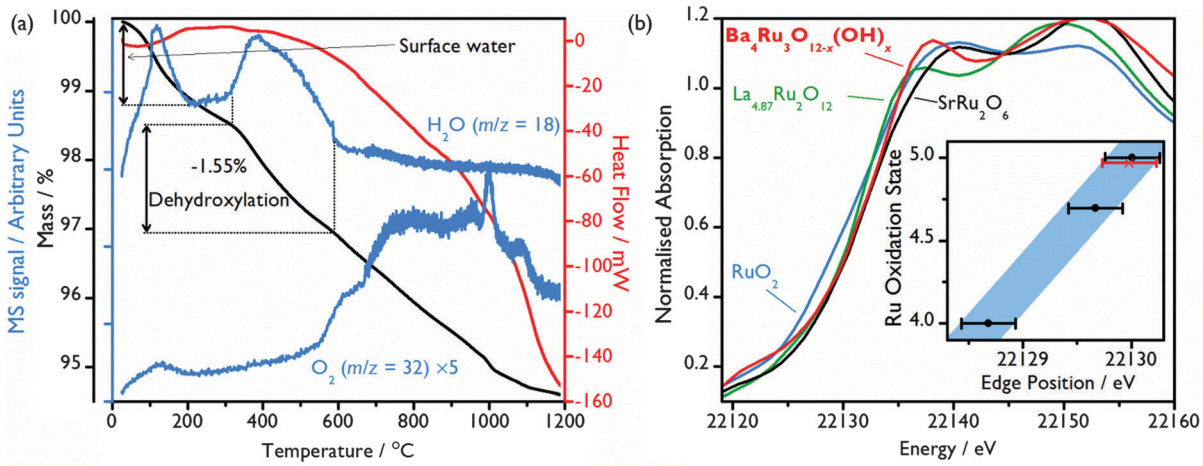

Fig. 3 (a) TGA-DSC under N_2 flow (heating rate 10 °C min^{-1}) with *in situ* MS signals associated with H_2O (*m/z* = 18) and O_2 (*m/z* = 32, multiplied by 5 for clarity). (b) Normalised Ru K-edge XANES spectrum of $Ba_4Ru_3O_{10.2}(OH)_{1.8}$ compared to reference spectra of $Ru^{(IV)}O_2$, $La_{4.87}Ru^{(4.70)}{}_2O_{12}$ and $SrRu^{(V)}{}_2O_6$. Inset shows a plot of Ru average oxidation state *vs.* edge position (measured where normalised absorption = 0.5). Black points correspond to reference samples, with a linear fit (blue, 0.5 eV wide, see text) which was then used to infer an average oxidation state from the $Ba_4Ru_3O_{10.2}(OH)_{1.8}$ (red point). Error bars were estimated from the core-hole broadening.

Open Access Article. Published on 07 April 2016. Downloaded on 2/10/2026 8:45:29 AM.
This article is licensed under a Creative Commons Attribution 3.0 Unported Licence.

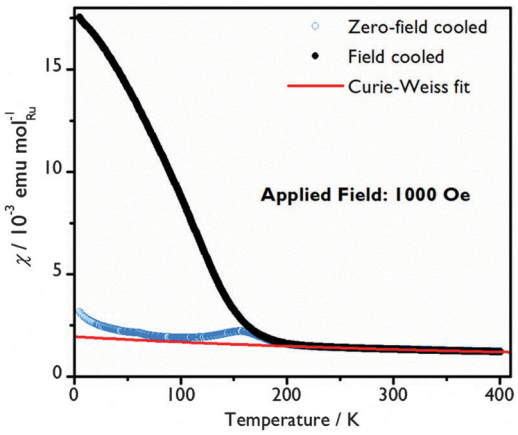

Fig. 4 Molar susceptibility as a function of temperature with a Curie–Weiss fit to the paramagnetic region of the field cooled data.

The system orders magnetically at $T_N = 200(5)$ K. A clear change in $d\chi_{FC}/dT$ that coincides with the minimum in the zero-field-cooled-warming $\chi(T)$ data may indicate a spin reorientation. At 5 K, the magnetisation increases almost linearly with applied field curve, with a moment of just 0.082(1) μ_B per Ru atom at 70 kOe indicating that the moments are principally aligned antiferromagnetically. A hysteresis in the $\chi(T)$ and $M(H)$ curves only seen below T_N reflects a small net magnetic moment and suggests that there may be a slight canting or a ferrimagnetic component to the spin arrangement at low temperature. A $|\theta|/T_N$ ratio of over 3, although still smaller than for some other Ru oxides,[20,32,33] reveals that in $Ba_4Ru_3O_{10.2}(OH)_{1.8}$ there is not a simple relationship between θ and T_N. Similar behaviour in other Ru oxides has been rationalised by considering the variation in the strength of the transfer energy and a crossover from localised to itinerant electrons.[34]

In summary, we have reported the hydrothermal preparation of a complex barium ruthenium oxyhydroxide using just two reagents and avoiding the presence of a second, competing phase. This illustrates how solution chemistry can be utilised to exert a high degree of control of both crystal structure and oxidation state in the solid state for 4d elements that are easily reduced to the elemental state under other synthesis conditions typically used. The use of a metal peroxide as a reagent provides a reactive metal source, and has potential in the discovery of other new phases under mild reaction conditions. $Ba_4Ru_3O_{10.2}(OH)_{1.8}$ is shown to be thermally unstable, with a structural transition and loss of hydroxide occurring at temperatures as low as 300 °C, suggesting it would be impossible to prepare by conventional solid-state synthesis. The hexagonal perovskite-type structure with hydroxide ions found close to vacant octahedral B-sites is a highly unusual (if not unique) H-environment in oxide chemistry. It may be noted that another hexagonal perovskite, $Sr_4Ru_3O_{12}$, previously reported to be synthesised under hydrothermal conditions (at 500 °C), contains partially occupied B-site octahedral sites but was characterised only by X-ray diffraction;[25] the presence of H would be undetectable by this method, and that phase could potentially be another example of a ruthenium oxyhydroxide. Our work suggests that the oxyhydroxide chemistry of 4d transition metal could be a fruitful place to discover materials with new structures and interesting magnetic and electronic properties, especially when mild solution synthesis allows access to phases not accessible at high temperatures.

We thank Johnson Matthey plc for their contribution to an EPSRC industrial CASE award to CIH, STFC for provision of neutron beamtime at ISIS *via* the GEM Xpress Access route, and Diamond Light Source for access to beamline B18.

References

1 K. Ishida, H. Mukuda, Y. Kitaoka, K. Asayama, Z. Q. Mao, Y. Mori and Y. Maeno, *Nature*, 1998, **396**, 658.
2 R. J. Bouchard and J. L. Gillson, *Mater. Res. Bull.*, 1972, **7**, 873–878.
3 C. I. Hiley, D. O. Scanlon, A. A. Sokol, S. M. Woodley, A. M. Ganose, S. Sangiao, J. M. De Teresa, P. Manuel, D. D. Khalyavin, M. Walker, M. R. Lees and R. I. Walton, *Phys. Rev. B: Condens. Matter Mater. Phys.*, 2015, **92**, 104413.
4 P. Khalifah, K. D. Nelson, R. Jin, Z. Q. Mao, Y. Liu, Q. Huang, X. P. A. Gao, A. P. Ramirez and R. J. Cava, *Nature*, 2001, **411**, 669–671.
5 J. A. Kurzman, L. M. Misch and R. Seshadri, *Dalton Trans.*, 2013, **42**, 14653–14667.
6 A. T. Ashcroft, A. K. Cheetham, J. S. Foord, M. L. H. Green, C. P. Grey, A. J. Murrell and P. D. F. Vernon, *Nature*, 1990, **344**, 319–321.
7 N. F. Atta, A. Galal and S. M. Ali, *Int. J. Electrochem. Sci.*, 2012, **7**, 725–746.
8 J. Darriet and M. A. Subramanian, *J. Mater. Chem.*, 1995, **5**, 543–552.
9 R. H. Mitchell, *Perovskites: Modern and Ancient*, Almaz Press, 2002.
10 S.-T. Hong and A. W. Sleight, *J. Solid State Chem.*, 1997, **128**, 251–255.
11 P. C. Donohue, L. Katz and R. Ward, *Inorg. Chem.*, 1965, **4**, 306–310.
12 T. Ogawa and H. Sato, *J. Alloys Compd.*, 2004, **383**, 313–318.
13 F. Grasset, C. Dussarrat and J. Darriet, *J. Mater. Chem.*, 1997, **7**, 1911–1915.
14 F. Grasset, M. Zakhour and J. Darriet, *J. Alloys Compd.*, 1999, **287**, 25–31.
15 P. D. Battle, S. H. Kim and A. V. Powell, *J. Solid State Chem.*, 1992, **101**, 161–172.
16 P. Lightfoot and P. D. Battle, *J. Solid State Chem.*, 1990, **89**, 174–183.
17 C. Mallika and O. M. Sreedharan, *J. Alloys Compd.*, 1993, **191**, 219–222.
18 D. E. Bugaris and H.-C. zur Loye, *Angew. Chem., Int. Ed.*, 2012, **51**, 3780–3811.
19 R. J. Darton, S. S. Turner, J. Sloan, M. R. Lees and R. I. Walton, *Cryst. Growth Des.*, 2010, **10**, 3819–3823.
20 C. I. Hiley, M. R. Lees, J. M. Fisher, D. Thompsett, S. Agrestini, R. I. Smith and R. I. Walton, *Angew. Chem., Int. Ed.*, 2014, **53**, 4423–4427.
21 C. Dussarrat, J. Fompeyrine and J. Darriet, *Eur. J. Solid State Inorg. Chem.*, 1994, **31**, 289–300.
22 V. Favre-Nicolin and R. Cerny, *J. Appl. Crystallogr.*, 2002, **35**, 734–743.
23 A. C. Larson and R. B. Van Dreele, Los Alamos National Laboratory Report LAUR, 1994, 86–748.
24 B. H. Toby, *J. Appl. Crystallogr.*, 2001, **34**, 210–213.
25 C. Renard, S. Daviero-Minaud, M. Huve and F. Abraham, *J. Solid State Chem.*, 1999, **144**, 125–135.
26 S. A. J. Kimber, M. S. Senn, S. Fratini, H. Wu, A. H. Hill, P. Manuel, J. P. Attfield, D. N. Argyriou and P. F. Henry, *Phys. Rev. Lett.*, 2012, **108**, 217205.
27 J. R. Neilson, J. A. Kurzman, R. Seshadri and D. E. Morse, *Inorg. Chem.*, 2011, **50**, 3003–3009.
28 W. D. Birch, A. Pring, A. Reller and H. Schmalle, *Naturwissenschaften*, 1992, **79**, 509–511.
29 I. Arčon, A. Benčan, A. Kodre and M. Kosec, *X-Ray Spectrom.*, 2007, **36**, 301–304.
30 K. Sardar, E. Petrucco, C. I. Hiley, J. D. B. Sharman, P. P. Wells, A. E. Russell, R. J. Kashtiban, J. Sloan and R. I. Walton, *Angew. Chem., Int. Ed.*, 2014, **53**, 10960–10964.
31 G. Bunker, *Introduction to XAFS: A Practical Guide to X-ray Absorption Fine Structure Spectroscopy*, Cambridge University Press, 2010.
32 P. D. Battle and W. J. Macklin, *J. Solid State Chem.*, 1984, **52**, 138–145.
33 J. Darriet, F. Grasset and P. D. Battle, *Mater. Res. Bull.*, 1997, **32**, 139–150.
34 P. D. Battle, J. B. Goodenough and R. Price, *J. Solid State Chem.*, 1983, **46**, 234–244.

 This journal is © The Royal Society of Chemistry 2016